

Barium Depletion in the NSTAR Discharge Cathode After 30,000 Hours of Operation

James E. Polk*, Angela M. Capece†, Ioannis G. Mikellides‡, Ira Katz§

Jet Propulsion Laboratory, California Institute of Technology, M/S 125-109

4800 Oak Grove Drive, Pasadena, CA 91109

Dispenser hollow cathodes rely on a consumable supply of barium released by impregnant materials in the pores of a tungsten matrix to maintain a low work function surface. Examinations of cathode inserts from long duration ion engine tests show deposits of tungsten at the downstream end that appear to block the flow of barium from the interior. In addition, a numerical model of barium transport in the insert plasma indicates that the barium partial pressure in the insert may exceed the equilibrium vapor pressure of the dominant barium-producing reaction, and it was postulated previously that this would suppress barium loss in the upstream part of the insert. New measurements of the depth of barium depletion from a cathode insert operated for 30,352 hours reveal that barium loss is confined to a narrow region near the downstream end, confirming this hypothesis.

I. Introduction

State-of-the-art hollow cathodes consist of a porous tungsten tube (the insert), which is contained in a refractory metal cathode tube with an orifice plate on the downstream end. A small fraction of the thruster propellant is injected through the hollow cathode, and the orifice serves to increase the internal pressure in the insert region. Electron emission from the inner surface maintains an internal plasma which heats the insert to the required operating temperature and helps conduct the current into the main discharge. A heater surrounding the cathode is used to preheat it prior to ignition.

A low emitter operating temperature is achieved by maintaining a layer of adsorbed oxygen and barium atoms that reduces the surface work function. In state-of-the-art impregnated cathodes Ba and BaO are supplied by barium calcium aluminate source material (the impregnant) incorporated in the pores of the tungsten. Gaseous Ba and BaO are released in interfacial reactions between the tungsten matrix and the impregnant, producing a temperature-dependent vapor pressure of these species inside the pores. The Ba and BaO then migrate to the surface by Knudsen flow and surface diffusion on the pore walls. In vacuum dispenser cathodes Ba adsorbates lost by evaporation are replenished by Ba and BaO through surface diffusion from the pores and most of the vapor flow from the pores is lost. In gas discharges, the vapor in the discharge may be transported back to the cathode surface, offering another path for replenishing Ba lost by desorption.

Near the surface, products of the impregnant reactions escape to the exterior through the pores, allowing the reactions to proceed to completion. Eventually, relatively stable tungstates are produced and production of volatile species in that region ceases. The reaction front proceeds into the insert as reactants nearer the surface are consumed and the porosity of the impregnant increases due to loss of volatile materials. The region behind the reaction front is depleted in barium and the depth of this depletion layer has been characterized in some cathode tests¹ as an indicator of remaining useful life.

Hollow cathodes are subject to a number of potential failure mechanisms. External erosion by high energy ions created downstream of the orifice has been observed in a number of tests²⁻⁴ and is the focus

*Principal Engineer, Propulsion and Materials Engineering Section, Associate Fellow AIAA

†Graduate Student, GALCIT, California Institute of Technology, Student Member AIAA

‡Senior Engineer, Propulsion and Materials Engineering Section, Senior Member AIAA

§Principal Engineer, Propulsion and Materials Engineering Section, Senior Member AIAA

of experiments and modeling discussed elsewhere.^{5,6} Damage to the emitting surface due to poisoning by reactive gases or buildup of bulk tungstate layers due to reactive impurities is another potential failure mode.⁷⁻⁹

Insert life is ultimately limited by the barium supply in the impregnant. When the barium supply rate from the interior or from the gas phase drops below the rate at which adsorbed atoms are lost from the surface by desorption, the surface coverage drops and the work function rises.¹⁰ The cathode eventually becomes impossible to ignite or cannot be heated to the temperatures needed for the required electron current density.

Finally, tungsten transport has been observed in many extended hollow cathode tests.^{2,4,10,11} Impregnated cathode temperatures are not high enough to cause significant evaporation of the tungsten matrix, so these processes are undoubtedly due to formation and subsequent dissociation of volatile tungsten compounds. No failures have been attributed to this mechanism, but it could potentially lead to cathode failure. Reduction in the cathode orifice diameter by deposition of tungsten eroded from internal surfaces could increase the operating temperature or prevent cathode ignition, and deposits of tungsten on the emitter surface appear to limit barium flow through the tungsten matrix.¹²

A combination of experiments and modeling is being used to develop the analytical capability to assess cathode failure risk due to barium depletion. In previous work^{12,13} detailed examinations of discharge cathode inserts from two long duration tests were reported. The 8200 hour Life Demonstration Test (LDT) was performed with a 30-cm engineering model thruster similar to that flown on the Deep Space 1 (DS1) mission^{14,15} under the NASA Solar Electric Propulsion (SEP) Technology Applications Readiness (NSTAR) Program.² A subsequent Extended Life Test (ELT) was performed with the DS1 flight spare NSTAR thruster, ultimately accumulating 30,352 hours of operation at several different throttle levels.³ Analysis of these inserts revealed dense deposits of tungsten at the downstream end of the insert and evidence that they blocked off the pores and prevented flow of barium from under the zone responsible for most of the electron emission. Despite this, the cathodes operated properly and exhibited no evidence of performance degradation.

A model of barium transport in the hollow cathode plasma^{12,13} showed that barium is very effectively recycled in the discharge. Barium emitted from the insert upstream of the tungsten shell blocking flow at the downstream end is ionized in the intense xenon plasma and pushed down to the surface by the electric field. An unexpected result of the numerical model was that over much of the length of the insert the neutral barium partial pressure exceeds the equilibrium pressure of the dominant barium-producing reaction. We proposed that this would suppress the impregnant decomposition reactions in these areas and prevent barium loss from the interior. The model predicted that barium was only supplied to the discharge from a narrow region just upstream of the tungsten shell blocking flow in the electron emission zone.

In this paper we present new experimental results from further examination of the ELT discharge cathode confirming that barium depletion occurs only in this narrow region.

II. Dynamics of Barium Depletion in Hollow Cathode Emitters

The discharge cathode in the LDT operated for a total of 8200 hours at a xenon flow rate of 3.7 sccm and a current that ranged from 13 to 15.2 A. Details of the post-test analyses of the insert and cathode assembly were reported previously.^{2,12} Here we summarize the key observations and report new measurements of the barium depletion depth as a function of position along the emitter.

Changes in the emitter geometry were characterized with laser profilometry and imaging in a scanning electron microscope (SEM). Figure (1) shows the surface profiles measured on the LDT insert and a control insert that had never been operated. The LDT discharge cathode profile exhibits erosion over 15 mm at the downstream end, with more severe erosion in the first 4-5 mm. Up to 100 μm of the tungsten matrix were lost at the tip.

SEM photomicrographs of the emitter surface show a combination of erosion and redeposition of tungsten at the downstream end. Photomicrograph I illustrates the appearance of the virgin porous tungsten structure from an unoperated insert. In comparison, the images from the LDT cathode reveal a dense growth of

vapor-deposited tungsten crystals at the tip which covers the tungsten pores. Tungsten deposits are found in the surface pores over the rest of the eroded region, although it is not clear from the SEM images if these deposits close off the surface as they appear to at the tip. The image at 10 mm shows a surface which is similar to that of an undisturbed insert. The erosion and subsequent redeposition of tungsten leads to a significant restructuring of the porous tungsten matrix at the downstream end.

The reduction of barium flux from the insert by tungsten deposits and the finite barium partial pressure are incorporated in a numerical model of barium transport in the hollow cathode discharge. This model was used to calculate the net barium flow from the insert and the resulting depletion depth as a function of time to compare with the experimental results. The barium transport model has been described in detail previously,¹² but we summarize the major features here briefly and describe improvements to the barium flux model and how the barium loss is integrated to determine depletion depths. The initial focus of the modeling is on barium because this is the dominant species produced by the insert.⁷ Barium transport is strongly influenced by the xenon plasma; the electron density and temperature control the ionization of barium, the electric field in the xenon plasma and collisions with xenon and xenon ions control the diffusion of barium. However, barium atom and ion densities are so low they do not significantly modify the charge density or temperature in what is primarily a xenon discharge. This allows us to separate the problem into two parts, and use the major species parameters predicted by a xenon discharge model as fixed quantities in the solution of the minor species transport equations.

The barium flow in the insert plasma is modeled using the species momentum and continuity equations assuming that viscous and magnetic field effects are negligible, that the phenomena of interest are sufficiently slow, i.e. there are no high frequency phenomena and fluid acceleration is small compared to the force terms, and that collisions between barium ions and other minor species (such as barium) are sufficiently rare that they can be neglected.

The results of the xenon plasma simulation for the NSTAR cathode at a discharge current of 13.3 A and a xenon flow rate of 3.7 sccm are displayed in Fig. (2). Figure (2a) shows the neutral flow field. Because of the small orifice, the neutral density is relatively high ($\sim 10^{22} \text{ m}^{-3}$). The density drops rapidly in a small region near the orifice because of flow out of the cathode and consumption of neutrals in the strong ionization zone at the downstream end of the insert. The streamlines reveal two sources of neutral gas; the upstream inlet and the return flow of ions neutralized on the walls. The streamlines from both sources converge on the orifice. Figures (2b) and (2c) illustrate the electron current transport and resultant plasma heating. The streamlines represent the electron current. As Fig. (2c) shows, the emitter temperature is strongly peaked at the downstream end and electron emission is confined to a region about 4 mm long near the orifice plate. The streamlines show that the electron flow converges on the orifice and resistive heating from the high current density results in a peak in the electron temperature of about 1.85 eV in the orifice. Further upstream the plasma potential is low and electrons can penetrate from the plasma to the insert surface, resulting in net electron flow to the insert.

The plasma density distribution and resulting ion flow are shown in Fig. (2d). The high electron temperature near the orifice leads to a peak plasma density of $\sim 10^{21} \text{ m}^{-3}$ at the downstream end of the insert. Ions created in this ionization zone flow out radially and upstream, as shown by the ion current streamlines. Xenon ions created here are neutralized on the walls and return to the discharge as neutrals, as shown by the neutral flow streamlines in Fig. (2a).

The experimental observations indicate that the restructuring of the tungsten in the eroded zone alters the permeability, restricting barium flow to the surface. Based on the measured depletion depths, we assumed that the pores were completely blocked for the first 2.5 mm at the downstream end, corresponding to a permeability of zero, and that the permeability varied linearly from zero to unity, corresponding to the flow resistance of an undisturbed region, over the insert from 2.5 mm to 4 mm from the tip. The barium plasma simulation results are shown in Fig. (3). The mean free path for barium atom ionization $\lambda_{mfp}^{iz} = u_{t,Ba}/\nu_{Ba}^{iz}$ based on the barium atom thermal velocity $u_{t,Ba} = (8kT_h/\pi m_{Ba})^{1/2}$ and the ionization frequency was calculated using the electron density and temperature profiles and is plotted in Fig. (3a). The mean free path for ionization upstream of the dense plasma region is on the order of meters, but drops to less than 0.1 mm near the orifice. Barium atoms that drift into the dense xenon plasma have a high probability of being ionized.

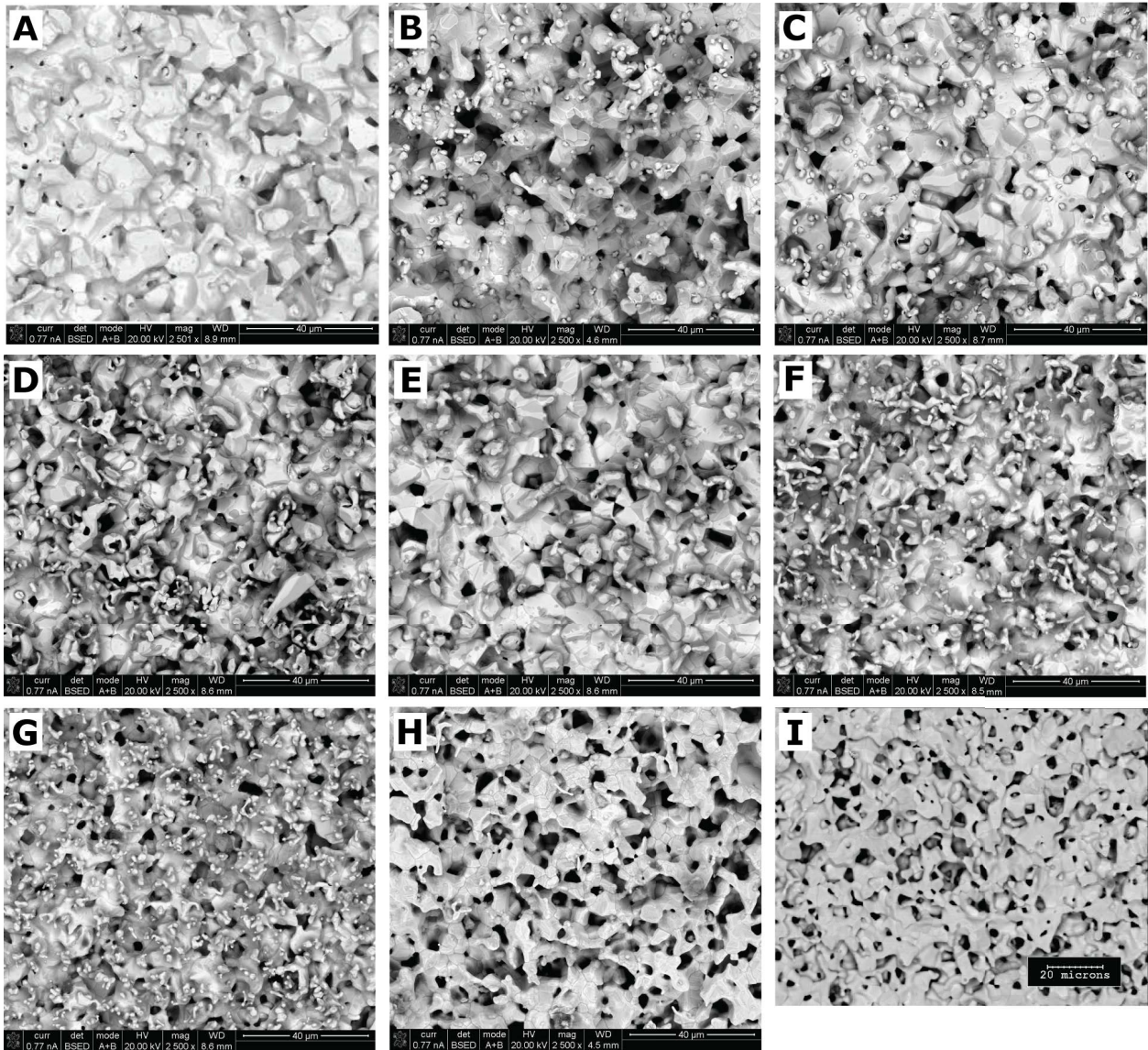
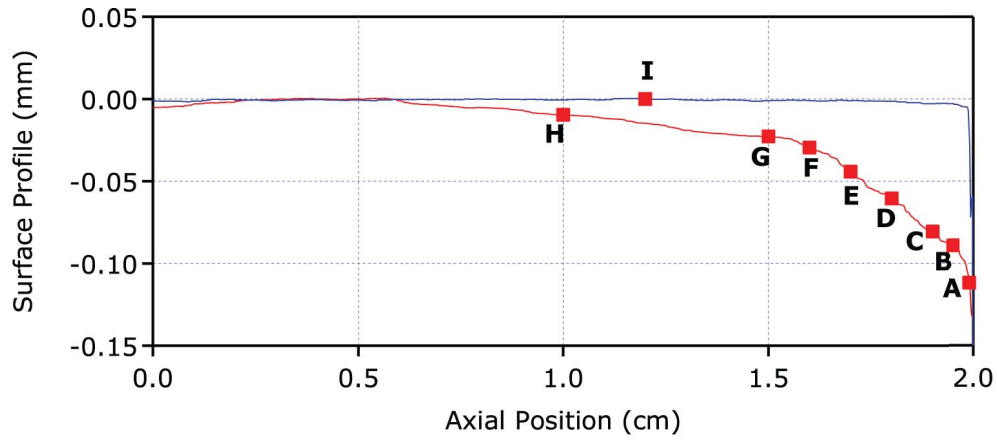
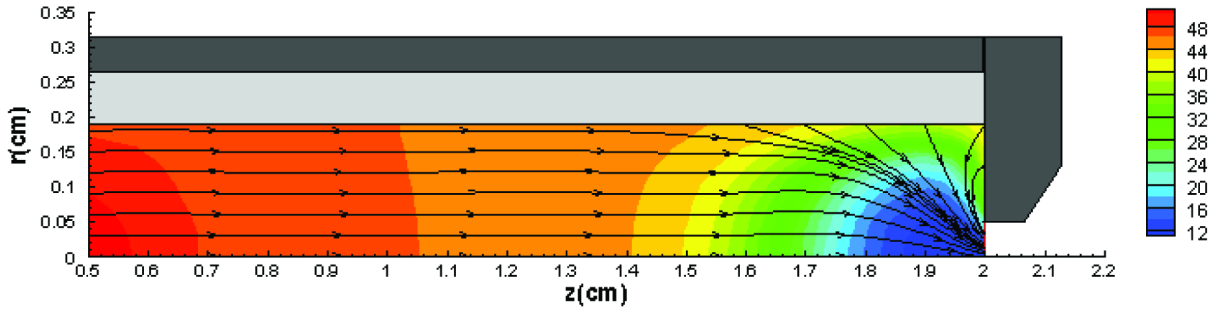
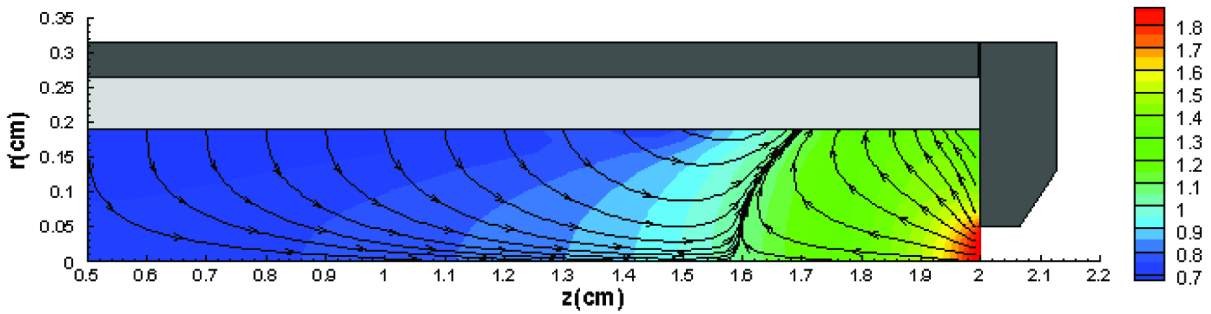


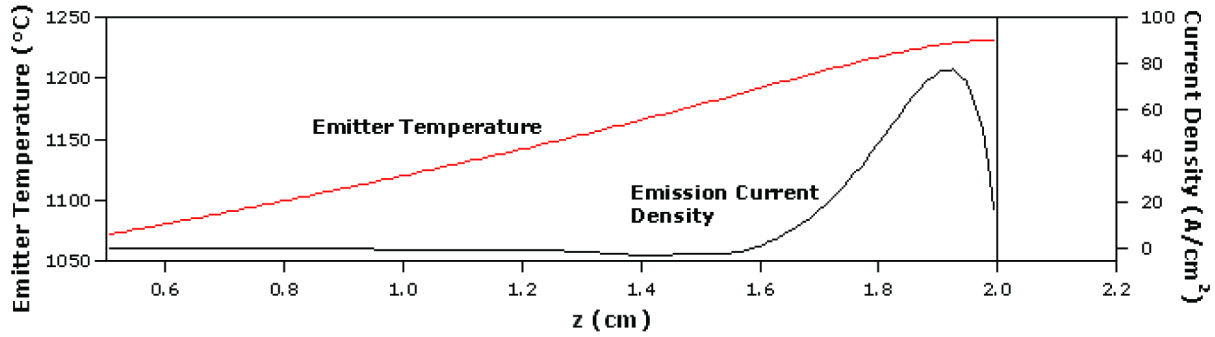
Figure 1. Profiles of the cathode emitter surface compared to an unused insert and photomicrographs showing the surface structure.



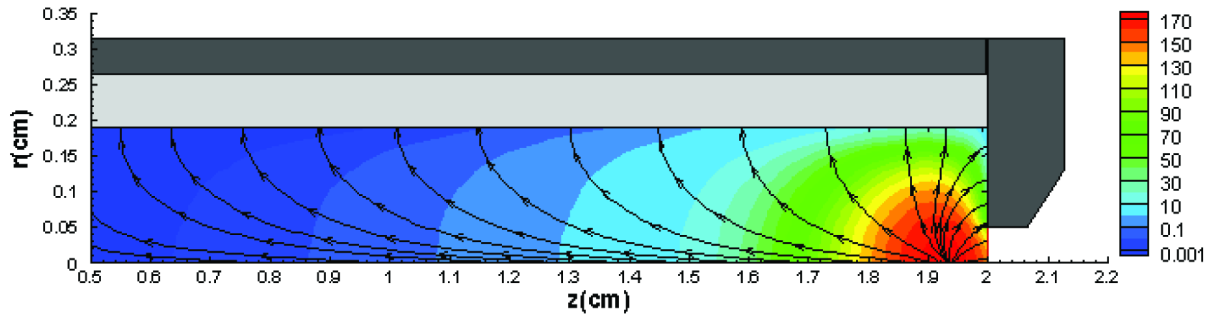
(a) Xenon neutral density contours, $n_{Xe}/10^{21}$ (m^{-3}) and neutral flux streamlines.



(b) Electron temperature contours (eV) and electron current streamlines.

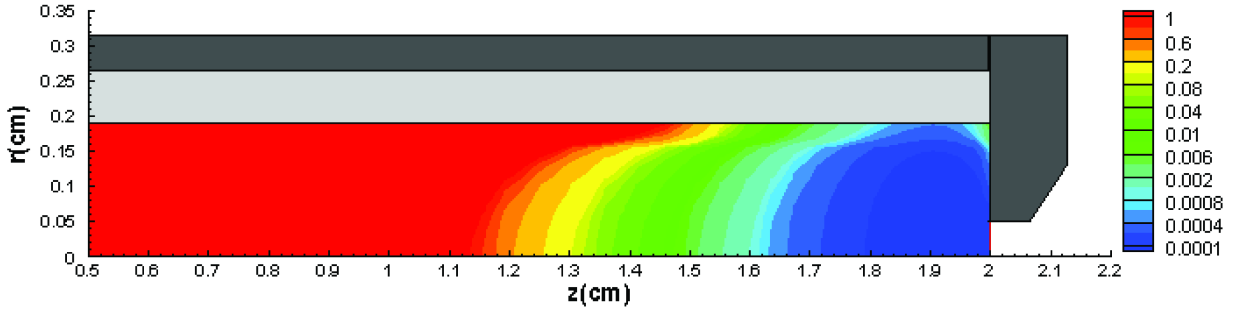


(c) Emitter temperature profile and electron emission current density.

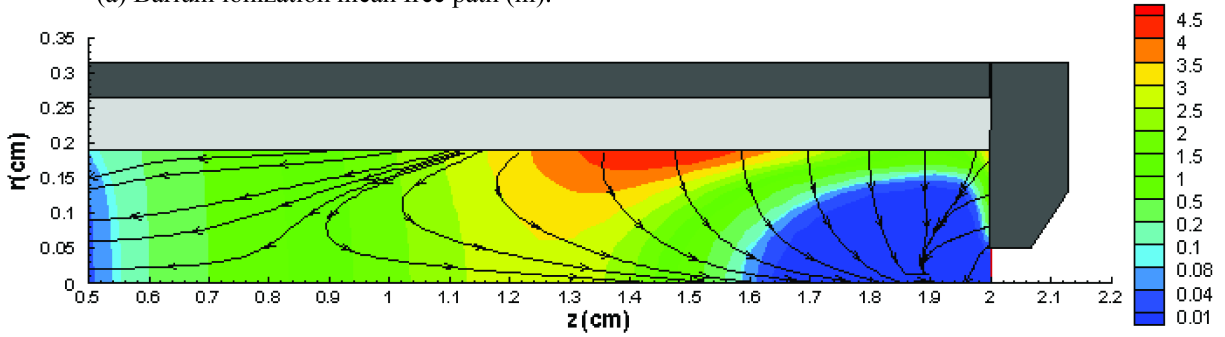


(d) Plasma density, $n_e/10^{19}$ (m^{-3}) and ion current streamlines.

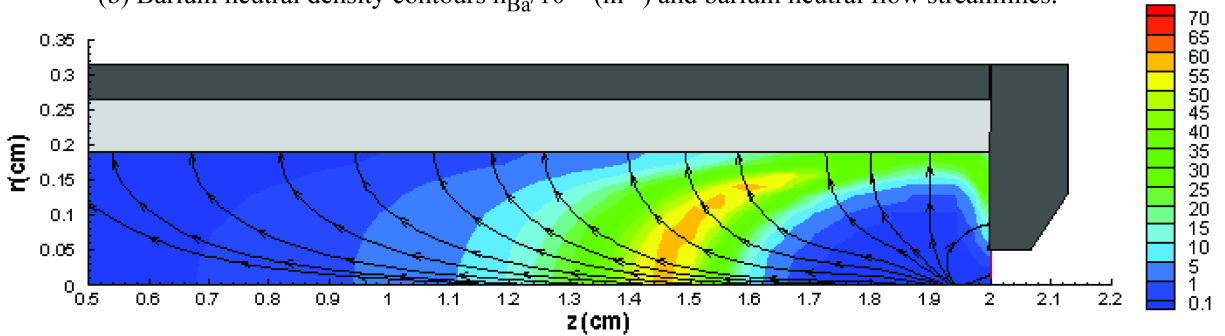
Figure 2. Xenon plasma solution for the NSTAR discharge hollow cathode at the full power operating point.



(a) Barium ionization mean free path (m).



(b) Barium neutral density contours $n_{\text{Ba}}/10^{16} \text{ (m}^{-3}\text{)}$ and barium neutral flow streamlines.



(c) Barium ion density contours $n_{\text{Ba}^+}/10^{14} \text{ (m}^{-3}\text{)}$ and barium ion flow streamlines.

Figure 3. Barium plasma solution for the NSTAR discharge hollow cathode at the full power operating point.

Figure (3b) shows the neutral barium flow field. The barium neutral density peaks at $\sim 4.5 \times 10^{16} \text{ m}^{-3}$ near the emitter surface at a point 0.5-0.6 cm upstream of the orifice plate and in the corner between the emitter and the orifice plate. The density decreases by up to two orders of magnitude at the upstream end of the insert and drops to near zero in the ionization zone near the orifice. All barium neutrals ultimately originate in the insert. Barium ions are neutralized on the walls and return to the interior as neutrals, providing a second source of neutral gas. There are two sinks for barium neutral gas—the cold surfaces upstream of the emitter where barium condenses and the ionization zone where neutrals are consumed in ionizing reactions. The neutral density is so low near the orifice that the neutral loss rate through the orifice is negligible. The steep neutral barium density gradient surrounding the ionization zone is sustained by a balance between the pressure gradient and the drag force associated with collisions between barium atoms and neutral xenon atoms.¹³

The barium ion density and flow streamlines are shown in Fig. (3c). The barium ion density is near zero inside the dense xenon plasma near the orifice and peaks in a relatively thin ionization front surrounding that zone. As Figures (3a) and (3b) indicate, neutral barium flowing toward the intense xenon plasma is ionized at the periphery. The barium ion streamlines show that the ions generated in the ionization zone flow outward and ultimately strike the emitter or the orifice plate, where they are neutralized and re-emitted

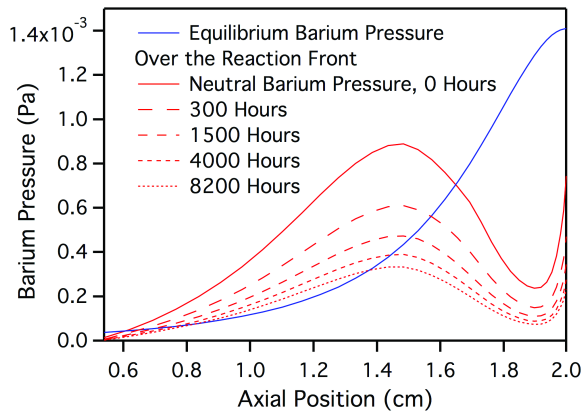
as barium atoms. The steady state barium ion density distribution is the result of a more complex balance of forces.¹³

The time-dependent model results for the measured temperature profile are plotted in Fig. (4). The calculated neutral barium partial pressure near the emitter is compared to the equilibrium barium pressure over the reaction zone in Fig. (4a). The equilibrium vapor pressure profile follows the cathode temperature profile, increasing monotonically in the downstream direction. The axial neutral pressure distribution first rises in the downstream direction, then drops where the electron density and temperature peak, due to ionization. Although barium flow from the emitter is set to zero over 2.5 mm at the downstream end of the insert, the neutral pressure rises again near the orifice plate in a small recirculation zone that is generated in the corner. The ambient barium pressure initially exceeds the equilibrium vapor pressure over much of the insert length, suppressing the reactions in the interior of the porous tungsten dispenser.

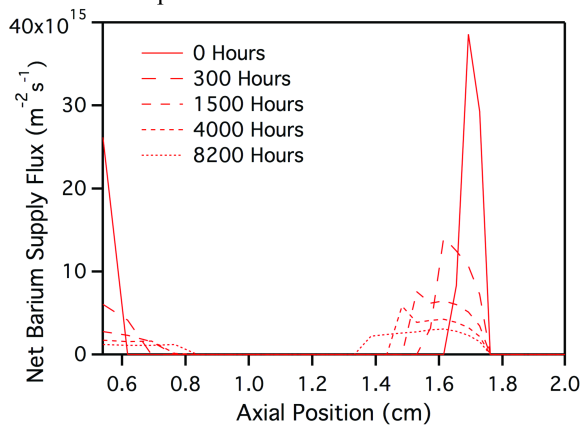
The decrease in neutral barium pressure with time apparent in Fig. (4a) is due to a reduction in the barium flux from the interior, as shown in Fig. (4b). The flux is initially peaked in the region between 1.6 and 1.75 cm. The distribution broadens with time as the neutral barium pressure falls below the equilibrium vapor pressure over the reaction front. Some barium emission also occurs at the upstream end where the partial pressure of barium falls below the equilibrium pressure for the reaction.

The recession of the reaction front into the interior with time is displayed in Fig. (4c). Barium depletion is initially restricted to the narrow region between 1.6 and 1.75 cm, but as more of the surface starts to emit barium, this profile also broadens. The maximum depth predicted for these conditions after 8200 hours of operation is about 130 μm just upstream of the region over which barium emission is set to zero. Some depletion at the upstream end can also be seen.

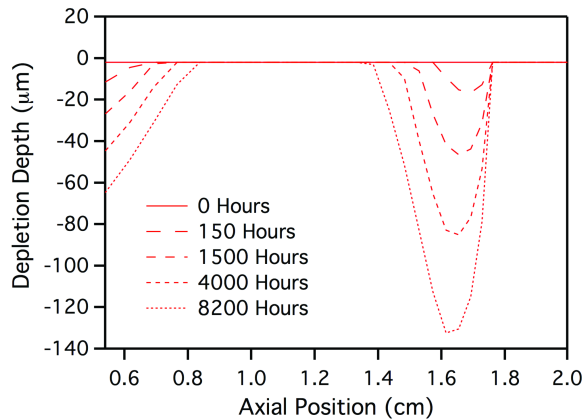
The simulation results are compared with the measured depletion depths in Fig. (5). When the barium partial pressure is equal to zero, eqn. (??) can be integrated over the total operating time to give the total depletion depth. The resulting depletion depth corresponding to operation in vacuum for 8200 hours is plotted as the lower dashed line in Fig. (5). These values are much larger than the measured values, highlighting the importance of the finite barium pressure in the discharge plasma in suppressing depletion.



a) Equilibrium barium pressure over the reaction front and profiles of the barium partial pressure in the insert plasma.



b) Variation in the profile of barium flux from the emitter due to depletion over time.



c) Depletion depth as a function of time.

Figure 4. Results of the time-dependent simulation for the nominal temperature profile.

The intermediate curve represents the results using the nominal temperature profile. It reproduces qualitatively the shape of the measured curve, with the maximum depletion depth upstream of the region with no barium emission and no depletion where the barium plasma pressure exceeds the equilibrium vapor pressure. This appears to confirm the proposed mechanism—suppression of barium production by the high barium partial pressure in the discharge. However, the predicted magnitude of the depletion depth is larger than the measured values by a factor of up to 2.5.

This discrepancy could be attributed to uncertainties in the equilibrium barium pressure for the impregnant

reduction reaction, the barium flow rates (the effective porosity of the porous structure, for instance), code predictions of the barium partial pressure in the discharge, or the cathode temperature. Sensitivity analyses indicate that temperature is the only parameter that can realistically account for this difference. For instance, if the barium flow rate from the interior was actually lower than the model described here would indicate, the magnitude of the depletion depth would be lower. However, lower flow rates would also reduce the partial pressure of barium in the insert plasma allowing more of the insert to emit barium and broadening the depletion depth profile. Conversely, if the actual equilibrium barium pressure over the reaction front was lower than that in the model, barium reactions would be suppressed over an even larger area and the depletion restricted to a narrower zone, but it would not change significantly the magnitude of the depletion depth.

The only parameter which affects both the magnitude of the depletion depth and the width of the profile is the temperature. If we assume that the temperature of the cathode is 70°C lower than the measured values, agreement between the model and the depth measurements is very good, as shown by the solid blue line in Fig. (5). The lower temperature reduces the rate of depletion, so the total depletion depth is lower. It simultaneously reduces the equilibrium barium pressure over the reaction front, so the reduced barium flow and resulting partial pressure in the insert plasma do not cause a broadening of the depletion depth profile. The depletion rate and the equilibrium vapor pressure are both exponentially dependent on the temperature, so a relatively small change in this parameter can explain the discrepancy between the measured and calculated depths. In comparison, the other parameters affect the rate and vapor pressure linearly, so much larger changes would have to be postulated to explain the difference.

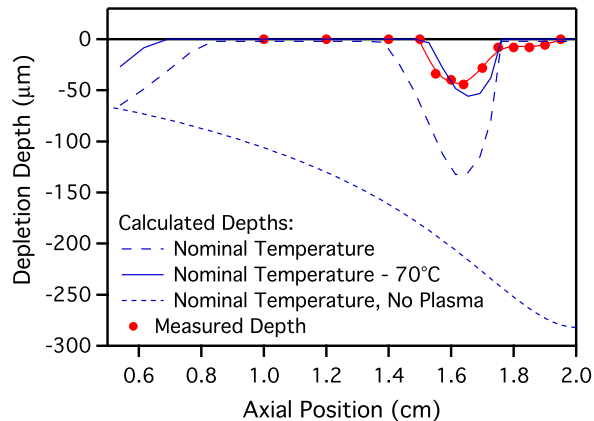


Figure 5. Comparison of measured depletion depths with simulation results.

A 70°C error in temperature is larger than would be expected given the uncertainties in the temperature measurements.⁷ However, temperature decreases of this magnitude over a period of several hundred hours have been observed at the beginning of long duration tests,⁷ so the measurements obtained in relatively short duration tests of a laboratory cathode that were used for the simulation may not be representative of the temperature in the LDT.

The picture that emerges from these data is that material is eroded from the insert, particularly in the emission site at the downstream end, but some fraction of it is redeposited locally. The local redeposition in the emission zone forms a much denser tungsten shell that impedes the flow of barium from the interior, inhibiting the reduction of the impregnant under the emission zone. Barium lost from the emitter by evaporation in this zone must be replenished through the gas phase by barium released further upstream.

Measurements of barium depletion depths on the LDT cathode revealed that barium losses were confined to a small region near the downstream end of the insert, confirming predictions made earlier on the basis of a numerical model of barium transport in the hollow cathode plasma.¹² The narrow depletion depth profile is the result of two effects. First, erosion and subsequent redeposition of tungsten at the downstream end restructures the porous tungsten matrix and reduces the permeability to barium flow from the interior. This effect prevents decomposition of the impregnant over the first few mm of the insert. Second, barium is recycled very efficiently in the insert plasma, and the barium partial pressure is relatively high in the discharge. Over much of the upstream part of the insert, the barium pressure exceeds the equilibrium vapor pressure of the reactants, suppressing the reaction and preventing depletion in those regions.

III. Measurements of Barium Depletion in the ELT Discharge Cathode Emitter

III.A. The NSTAR Extended Life Test

The NSTAR Extended Life Test was designed to identify unexpected failure modes, characterize the parameters which drive known failure mechanisms and determine the effect of engine wear on performance. In this test, a flight-model NSTAR ion engine was operated in a large vacuum facility for a total of 30,352 hours over a range of throttle conditions which are summarized in Table (1). The discharge voltage varied by less than 1 V in any single test segment. It decreased by about 1.3 V between the first and second TH15 segments, but the value during the third TH15 segment was about the same as that in the second segment. The time required to ignite the cathode with constant heater power and starting voltage was unchanged in 30,352 hours. The discharge voltage and ignition behavior indicate that the discharge cathode emitter was healthy throughout the entire wear test. XXX-Add blurb about keeper voltage. Over the course of the test the keeper electrode eroded due to high energy ion bombardment, and by 29,000 hours the keeper orifice plate had disappeared. The cathode orifice plate also experienced some erosion on the periphery, but remained structurally sound with little change in the orifice geometry. Details of the test facility, thruster hardware, operating conditions, engine performance and post-test analyses results are provided elsewhere.[?]

Test Segment	1	2	3	4	5	6	7
Throttle Level	TH12	TH15	TH8	TH15	TH0	TH15	TH5
Engine Power (kWe)	2.0	2.3	1.5	2.3	0.5	2.3	1.1
Duration (hrs)	447	4246	5758	5166	5689	4400	3494
Cathode Flow Rate (sccm)	2.8	3.7	2.42	3.7	2.42	3.7	2.42
Discharge Current (A)	11	14.5	8.5	15	5	15	6.5

Table 1. Discharge cathode test conditions in the Extended Life Test

III.B. Experimental Approach

The cathode insert from the 30,352 hour ELT was fractured along its axis to allow inspection.⁴ In the investigation summarized here the insert was further analyzed to gain more insight into material transport and its effect on the emission zone. The profile of the interior surface was measured using a laser profilometer system with a resolution of less than 1 μm . The profilometer calibration was checked by scanning a series of steps made with precision ground ceramic blocks of different heights that had been rung onto an optical flat.

The surface morphology and internal porosity of the insert were characterized in examinations with a scanning electron microscope (SEM). The composition of the impregnant and various deposits was determined using energy-dispersive spectroscopy (EDS). One insert sample was potted to allow a fracture surface to be polished. This was done with very fine diamond abrasives wetted with kerosene to avoid removing impregnant material from the pores. SEM exams and EDS analysis were then used to characterize the cathode bulk. In particular, EDS analyses of individual impregnant grains as a function of depth were used to determine the extent of barium depletion in the impregnant material.

This approach differs from methods previously applied to determine barium depletion depths and provides much more reliable results. Element maps constructed using EDS scans over the cathode cross-section were employed in initial studies of the LDT discharge cathode¹² and by others.[?] These images are time-consuming to construct because the resolution and integration time must be very high to accumulate an adequate signal from the relatively small impregnant grains in an image, but can provide a good qualitative picture of the element distributions. An example of this approach is shown in Fig. (6). The image is a barium element map of a region on the cross-sectioned LDT discharge cathode insert approximately 0.8 mm long located just upstream of the tip. The right side is the electron emission zone on the inner diameter of the insert

and the left side is the outer diameter of the insert. The bright points are concentrations of barium in the tungsten matrix. The tungsten shows as a faint background in this image.

The barium-free zone where the insert was etched after impregnation is faintly visible on the left side, but has been mostly removed by erosion on the right. Quantitative measurements of the element distributions can be obtained in line scans across an image, but suffer from low signal-to-noise ratio. The signal-to-noise ratio can be improved by averaging across images, as shown in Fig. (6). The yellow line is the sum of the columns composing the image and represents the average barium signal strength at each radial location. The white trace is based on a similar analysis of the calcium element map. The tungsten background has been subtracted from these signals. On the left side of the image is an intermediate layer where the barium signal drops to about half that in the interior and the calcium signal drops nearly to zero. This is the zone from which impregnant material has been depleted by reactions with the tungsten. The space between the insert and the cathode tube was filled with a layer of BaO, which is undoubtedly the result of reaction products flowing out from this reaction zone. On the right side of the image a thin region with little or no impregnant is visible, but there is no depletion layer as on the left. The barium and calcium signals are uniform up to the tungsten layer. Upstream of the region with the heaviest erosion the depletion layer can be found on both surfaces of the cathode, although the layer thickness decreases with increasing distance upstream.

A different method used in initial studies of the ELT cathode⁷ also suffers from poor signal-to-noise ratio and do not appear to yield accurate quantitative measurements of the depletion depth as a function of position along the emitter. In this approach, regions of interest encompassing some number of impregnant grains in the pores of the tungsten matrix are defined at various depths, and the ratios of barium to tungsten concentration are determined using EDS scans. However, the nonuniform distribution of impregnant material in the matrix and the overwhelming concentration of tungsten result in large uncertainties. In addition, the number of measurements in both the axial and radial directions was insufficient to resolve the actual depletion boundary or the axial variation in depletion depth.

In this study, quantitative measurements were obtained using EDS analysis of individual impregnant grains visible in the polished cross section of the emitter. Figure (7) shows an example of an area near the emitter surface. The open pores in the etched region are visible in the top half of the image. In the lower half, the pores are filled with impregnant material.

The concentration of aluminum remains relatively constant over the insert interior because Al in the impregnant does not form volatile reaction products. It can therefore be used as an internal standard to determine relative concentrations of barium and calcium. Regions which are depleted in the volatile species Ba and Ca will have lower ratios of Ba or Ca peak area to Al peak area compared to those in regions with unreacted impregnant. The difference is quite obvious, as shown in Fig. (8). Regions in individual impregnant grains were identified on the SEM images and EDS spectra were obtained for those areas. Peak areas for the dominant Ba, Ca and Al lines in the spectra were calculated and used to form the ratios, which were then plotted as a function of the depth of the impregnant grain below the boundary defining the edge of the impregnated zone.

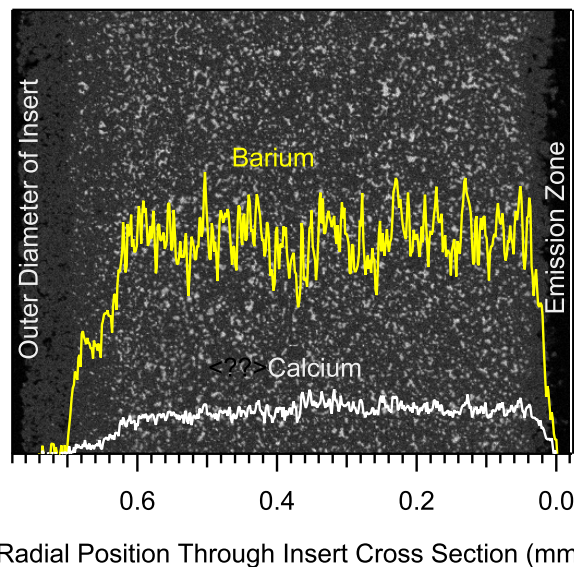


Figure 6. Barium element map and profiles for barium and calcium in a cross section of the LDT cathode.

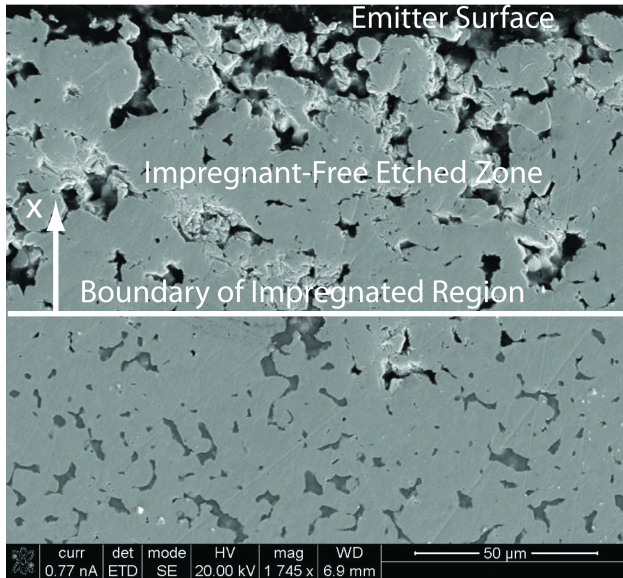


Figure 7. Photomicrograph of the insert cross section showing pores containing impregnant material (bottom of image) and the impregnant-free etched zone near the surface (top of image).

In this example, grains deeper than about $40\ \mu\text{m}$ have Ba/Al ratios of about 2.5 and Ca/Al ratios of 0.29. Grains near the surface have corresponding ratios of 0.75 and zero, reflecting a loss of volatile Ba and Ca reaction products. In some locations, the Ca/Al ratios in the interior were as high as 0.6, perhaps reflecting a nonuniform distribution of free CaO. Examining individual grains at different depths provided a relatively well-defined boundary for the depleted zone. The majority of grains above the boundary exhibited barium and calcium depletion, although isolated exceptions were found, probably in locations which did not have interconnected pores forming a path to the surface.

III.C. Experimental Results

The profiles of the insert inner surfaces are shown in Fig. (??). These are based on profilometer scans along the axis of the insert fragments which yielded the surface height above a flat reference plane on which the insert fragment rested. The height values were shifted so that zero height represents the original interior surface, and the erosion depth (or increase in inner radius of the cylindrical insert) is indicated by negative values. The original surface datum was clear in the control insert and the neutralizer insert, which exhibited very little internal erosion. For the discharge cathode inserts however, points near the upstream end where SEM exams showed surfaces that did not appear to be eroded or covered with deposits were assumed to be the original, uneroded surface. This is somewhat subjective, however, so the magnitude of the erosion depths indicated by negative values on the abscissa may be underestimated.

The control insert surface profile was flat to within $\pm 5\ \mu\text{m}$ except near the upstream end where the indicated height drops slightly, which represents an increase in the insert inner radius of about $15\ \mu\text{m}$. This feature is near the interface between the porous tungsten insert and a molybdenum ring that is brazed on the upstream end, and may be an artifact of machining. The LDT neutralizer insert profile is almost identical, except that it shows a smooth, filleted transition to the molybdenum ring. The LDT discharge cathode profile exhibits

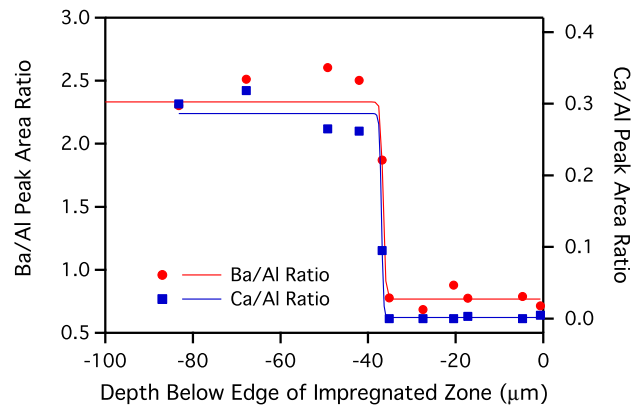


Figure 8. The boundary between unreacted impregnant and the near-surface depleted layer based on ratios of Ba and CaI peak areas to that of Al, which serves as an internal standard.

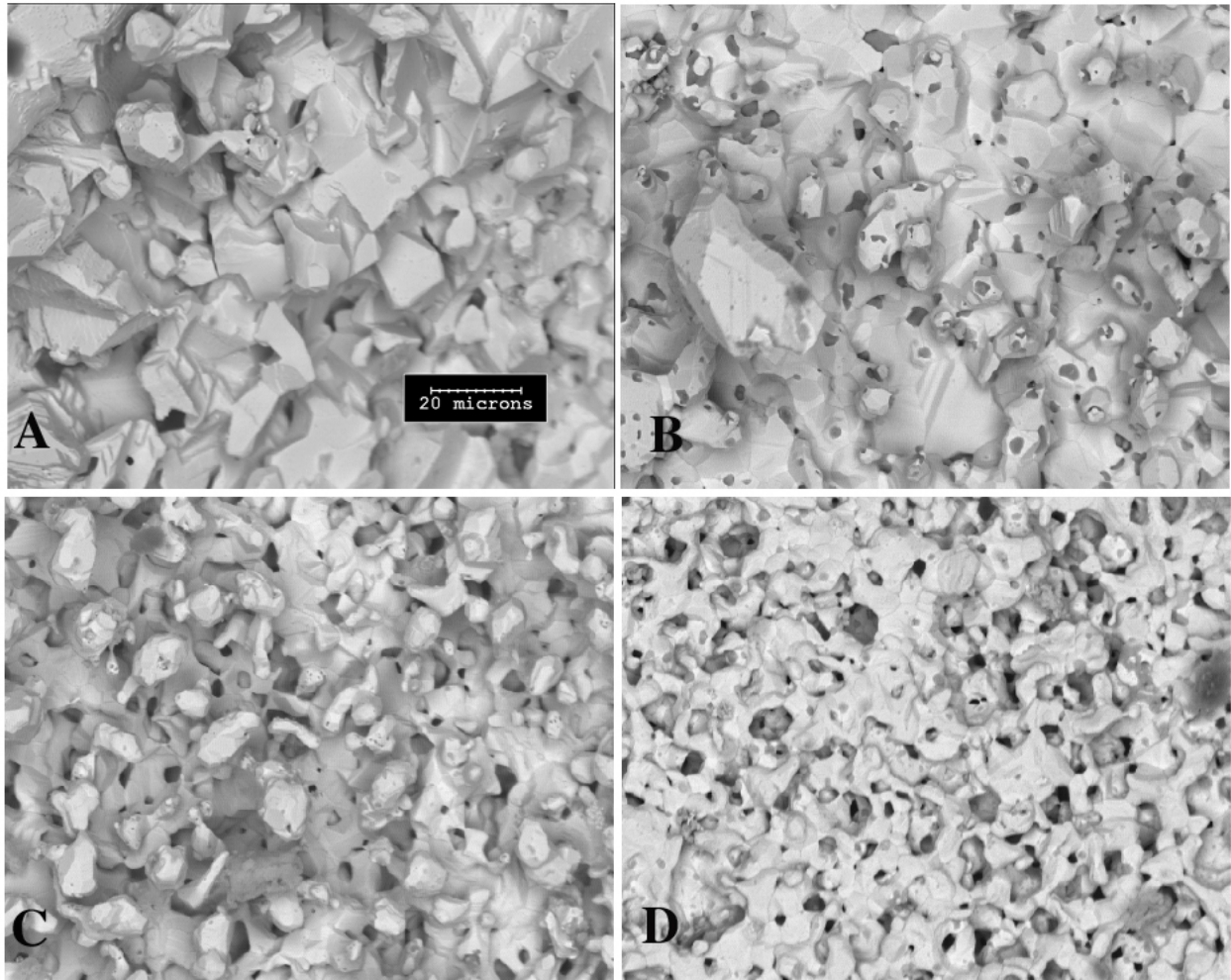
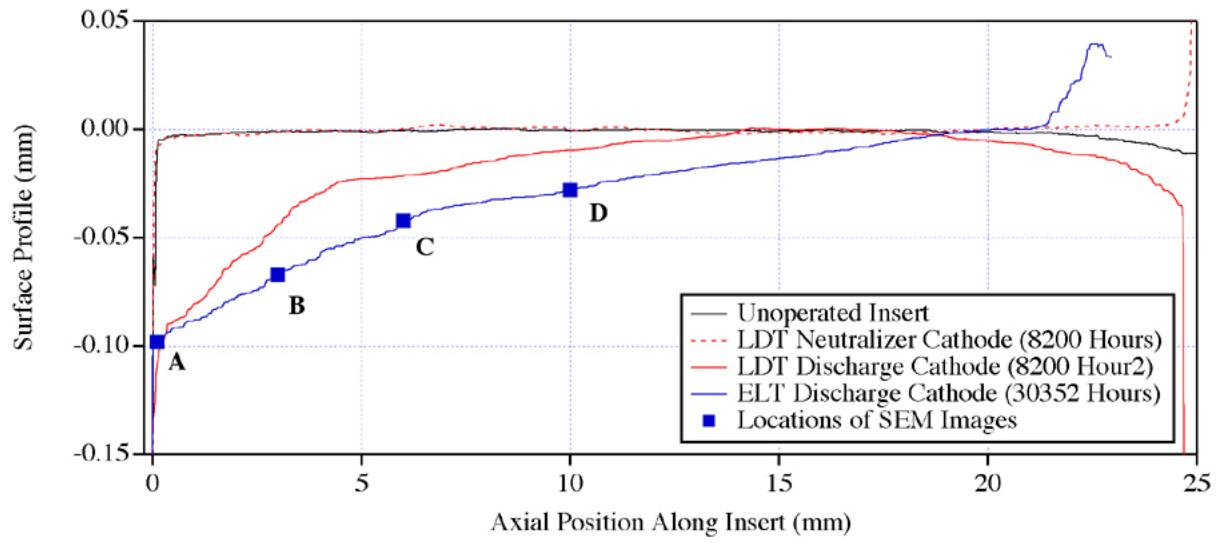


Figure 9. SEM images of the ELT discharge cathode insert inner surface.

erosion over 15 mm at the downstream end, with more severe erosion in the first 4-5 mm. Approximately 74 mg of tungsten was eroded from this region, which is equivalent to 4×10^{-4} moles with an average erosion rate of 1.5×10^{-9} g/cm²s. The radius of this insert is also larger near the upstream end. It is not clear if this is the same kind of feature seen in the control insert, or if it indicates another erosion site.

The ELT discharge cathode insert is qualitatively similar to the LDT insert at the downstream end, although the erosion is generally deeper and the transition in the slope of the eroded surface occurs at about 7 mm from the tip. The total erosion in the ELT insert was approximately 126 mg or 6.9×10^{-4} moles with an average erosion rate of 5.2×10^{-10} g/cm²s over the course of the test. Both profiles indicate a maximum eroded depth at the tip of 100 μ m, which yields a peak erosion rate of 1.4 – 5.2×10^{-9} g/cm²s. The ELT insert had thick deposits of barium compounds on the last 3 mm of the upstream end, which is seen in the profile as an increase in height of about 30–40 μ m over the original surface.

The morphology of the ELT discharge cathode insert varies considerably with position, as shown in Fig. (9). Photomicrographs A and B show tungsten crystals that were noted earlier⁴ and have been observed in many long duration tests.^{2,10,11} What is most striking about these photomicrographs is that they reveal a dramatic restructuring of the surface. This is evidently not only a site of erosion, but also of subsequent redeposition, resulting in a net recession of the surface accompanied by densification of the matrix. In this region the surface porosity is much lower than the original surface. Image C represents a transition from the region with crystalline deposits to the original porous structure. Image D shows that by 10 mm from the downstream end, the surface looks very similar to that of the unoperated insert, although the profile data indicate that net erosion has occurred here. With the exception of the thick barium deposits found on the upstream end of the insert, very little barium was observed on the surface.

The results of the depletion depth measurements are shown in Fig. (10). The blue line and filled circles represent the surface profile. Measurements of the etched layer thickness along the insert indicate that it is about 40 μ m deep except where it has been eroded at the downstream end. The insert profile was shifted so that the zero datum corresponds to the edge of the impregnated layer (below the etched region). As in the LDT insert, the barium loss was confined primarily to a narrow region just upstream of the emission zone. In the ELT insert this region extends from about 4 to 8 mm from the cathode tip, compared to 3 to 5 mm from the tip in the LDT insert, and it is about 3 times deeper. There is no depletion of barium from 2.5 to 4 mm or upstream of 8 mm. Unlike in the LDT insert, there is some barium depletion at the cathode insert tip.

Photomicrographs illustrating the distribution of barium in the different regions are shown in Figures (11)–(13). Figure (11) displays a region near the surface located 3 mm from the insert tip. A dense tungsten layer is visible at the surface with no evidence of the porosity found in the virgin matrix. The etched zone has apparently been completely obliterated by the combination of erosion and redeposition. EDS analysis of the impregnant grains visible below the tungsten shell indicated that most of them were undisturbed. Only a few grains nearest the surface exhibited the signature of barium depletion.

The image in Fig. (12) taken 6.5 mm from the tip is representative of the depleted region upstream of the emission zone. The open pores in the etched layer are visible at the top, and at this location the etched zone is about 30 μ m deep. The boundary between the undisturbed impregnant and the depleted region is shown below that. The grains identified with circles exhibited the reduced calcium and barium concentrations relative to aluminum that are characteristic of depletion. Those identified with rectangles produced EDS spectra with the nominal relative levels of barium and calcium. The boundary is at approximately 101 μ m below the surface. This figure illustrates the uncertainty in the measurements, which is on the order of ± 10 μ m. XXX-expand a little on this.

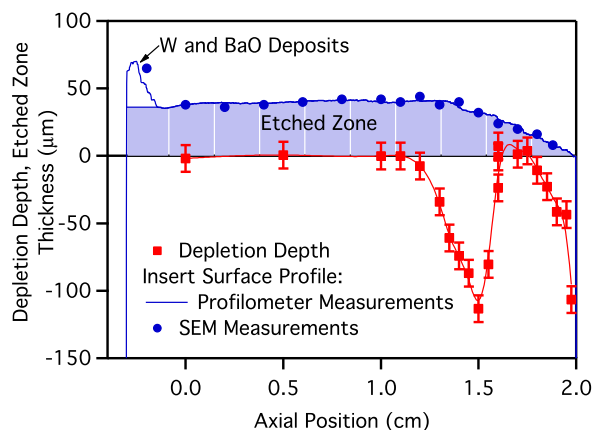


Figure 10. Measured thickness of the etched layer near the surface and depletion depth in the impregnated region beneath it. The zero line represents the boundary of the impregnated region.

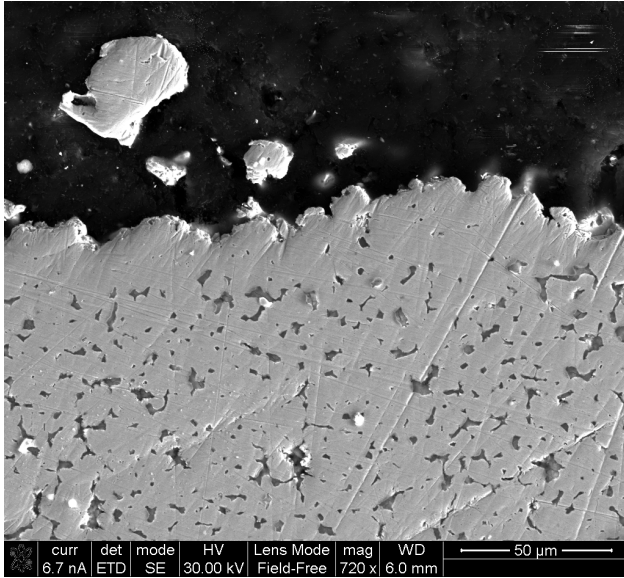


Figure 11. SEM image of the cathode cross section 3 mm from the tip showing the dense tungsten shell at the surface. The SEM image in Fig. (13) was taken 10 mm from the insert tip and is typical of the upstream portion of the insert. In this location, the etched layer is about $39\ \mu\text{m}$ thick. The impregnant grains in the pores below that all showed nominal relative concentrations of barium and calcium, indicating no depletion.

IV. Discussion and Conclusions

The insert analyses and modeling resulted in three main conclusions that have significant implications for hollow cathode lifetime. First, tungsten erosion and subsequent redeposition in the emission zone result in the formation of a dense tungsten shell with reduced porosity. This deposit inhibits barium flow from the interior and therefore suppresses the reaction, resulting in very little barium depletion under the primary electron emission zone. Despite this, hollow cathodes appear to function correctly for very

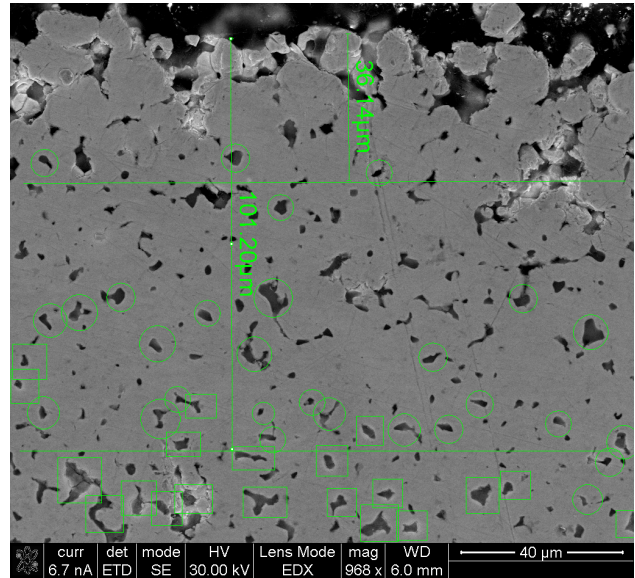


Figure 12. SEM image of the cathode cross section 6.5 mm from the tip showing the etched zone and depleted layer.

The barium transport model shows that barium in the downstream region can be very effectively supplied through the gas phase and will maintain adequate surface coverage in the emission zone for lifetimes on the order of those achieved in long duration tests. The key difference between hollow cathode gas discharges and vacuum dispenser cathodes is that hollow cathodes make much more efficient use of the barium supplied by the insert. Neutral barium from the insert is ionized in the intense xenon plasma, and the combination of the electric field and the drag from the xenon ion flow results in a high barium ion flux to the emitter surface. The ions are neutralized on the surface and return to the discharge to be ionized again. Because the upstream boundary is the only effective sink for barium (except under conditions in which barium can accumulate on the cathode surface; in the presence of oxidizing impurities for instance) a high barium partial pressure builds up at the downstream end.

The high barium partial pressure appears to suppress impregnant reduction reactions over most of the insert length. Barium is evidently supplied only from a narrow region where ionization reduces the neutral density below the equilibrium vapor pressure. This result is the most surprising, and perhaps the most uncertain because it relies on the relative values of thermochemical properties which are not well known. A careful

examination of the depletion profile along hollow cathodes from long duration wear tests could help confirm this conclusion. This is another example of self-regulation in hollow cathodes—the barium production rate increases until the pressure builds up sufficiently to suppress reactions over some length of the insert. This suggests that barium located upstream of the electron emission site is not wasted, but is critical to the operation of the discharge through gas phase resupply and, in fact, much of this supply is saved until it is needed. These improvements in understanding of barium transport processes indicate that models of cathode failure due to barium depletion that are based on vacuum dispenser cathode data are likely to be extremely conservative.

V. Acknowledgements

The authors would like to thank Jim Kulleck for his assistance with the scanning electron microscope. The research described in this paper was carried out by the Jet Propulsion Laboratory, California Institute of Technology, under a contract with the National Aeronautics and Space Administration. Reference herein to any specific commercial product, process, or service by trade name, trademark, manufacturer, or otherwise, does not constitute or imply its endorsement by the United States Government or the Jet Propulsion Laboratory, California Institute of Technology.

References

- ¹Shroff, A., Palluel, P., and Tonnerre, J., “Performance and Life Tests of Various Types of Impregnated Cathodes,” *Applications of Surface Science*, Vol. 8, 1981, pp. 36–499.
- ²Polk, J., Anderson, J., Brophy, J., Rawlin, V., Patterson, M., and Sovey, J., “The Results of an 8200 Hour Wear Test of the NSTAR Ion Thruster,” *35th Joint Propulsion Conference*, Los Angeles, CA, 1999, AIAA-99-2446.
- ³Sengupta, A., Brophy, J., and Goodfellow, K., “Status of the Extended Life Test of the DS1 Flight Spare Ion Engine after 30,352 Hours of Operation,” *40th Joint Propulsion Conference*, Fort Lauderdale, FL, 2004, AIAA-2004-4558.
- ⁴Sengupta, A., “Destructive Physical Analysis of Hollow Cathodes from the Deep Space 1 Flight Spare Ion Engine 30,000 Hr Life Test,” *29th International Electric Propulsion Conference*, Princeton, NJ, 2005, IEPC 2005-026.
- ⁵Mikellides, I., Katz, I., Goebel, D., and Jameson, K., “Driving Processes in the Orifice and Near-Plume Regions of a Hollow Cathode,” *41st Joint Propulsion Conference*, Sacramento, CA, 2006, AIAA-2006-5151.
- ⁶Jameson, K., Goebel, D., Mikellides, I., and Watkins, R., “Local Neutral Density and Plasma Parameter Measurements in a Hollow Cathode Plume,” *41st Joint Propulsion Conference*, Sacramento, CA, 2006, AIAA-2006-4490.
- ⁷Polk, J., “The Effect of Reactive Gases on Hollow Cathode Operation,” *41st Joint Propulsion Conference*, Sacramento, CA, 2006, AIAA-2006-5153.
- ⁸Polk, J., “Long and Short Term Effects of Oxygen Exposure on Hollow Cathode Operation,” *42nd Joint Propulsion Conference*, Cincinnati, OH, 2007, AIAA-2007-5191.
- ⁹Capece, A., Polk, J., and Shepherd, J., “Surface Characterization of Barium Tungstate Formation in Hollow Cathodes,” *Space Propulsion 2008 Conference*, Heraklion, Greece, 2008.
- ¹⁰Sarver-Verhey, T., “Destructive Evaluation of a Xenon Hol-

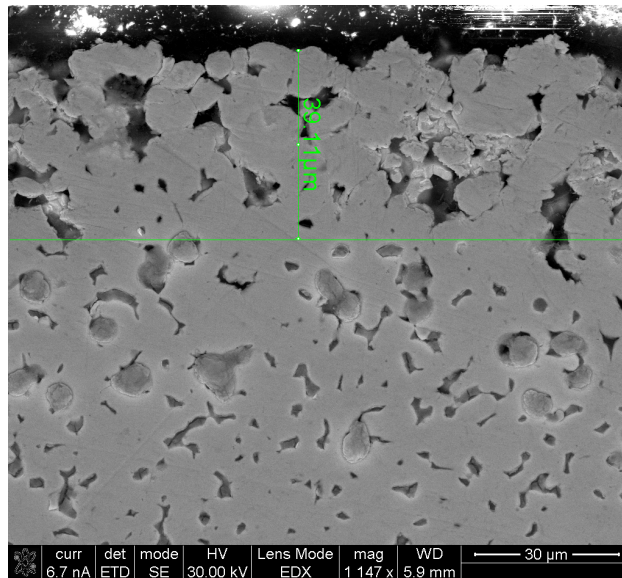


Figure 13. SEM image of the cathode cross section 10 mm from the tip showing the etched zone with no evidence of barium depletion below it.

low Cathode After a 28,000 Hour Life Test,” 34rd *Joint Propulsion Conference*, Cleveland, OH, 1998, AIAA-98-3482.

¹¹Verhey, T., “Microanalysis of Extended-Test Xenon Hollow Cathodes,” 27th *Joint Propulsion Conference*, Sacramento, CA, 1991, AIAA-91-2123.

¹²Polk, J., Mikellides, I., Katz, I., and Capece, A., “Tungsten and barium transport in the internal plasma of hollow cathodes,” *J. Appl. Phys.*, Vol. 105, 2009, pp. 113301.

¹³Polk, J., Mikellides, I., Katz, I., and Capece, A., “Dynamics of Barium Flow In Hollow Cathode Plasmas,” *JANNAF 6th MSS/4th LPS/3rd SPS Conference*, Orlando, FL, 2008, JANNAF-SPS-III-45.

¹⁴Brophy, J., “NASA’s Deep Space 1 Ion Engine,” *Rev. Sci. Inst.*, Vol. 73, No. 2, 2002.

¹⁵Polk, J., Brinza, D., Kakuda, R., Brophy, J., Katz, I., Anderson, J., Rawlin, V., Patterson, M., Sovey, J., and Hamley, J., “Demonstration of the NSTAR Ion Propulsion System on the Deep Space One Mission,” 27th *International Electric Propulsion Conference*, Pasadena, CA, 2001, IEPC-01-075.